This is the accepted manuscript made available via CHORUS. The article has been published as:

Quasiparticle and γ-band structures in ^{156}Dy

S. Jehangir, G. H. Bhat, J. A. Sheikh, S. Frauendorf, S. N. T. Majola, P. A. Ganai, and J. F. Sharpey-Schafer

Phys. Rev. C **97**, 014310 — Published 18 January 2018

DOI: 10.1103/PhysRevC.97.014310

Quasiparticle and γ-band structures in ^{156}Dy

S. Jehangir[1,2], G.H. Bhat[1,3,4], J.A. Sheikh[1,4], S. Frauendorf[5], S.N.T. Majola[6,7], P.A. Ganai[2] and J.F. Sharpey-Schafer[8]
[1]*Department of Physics, University of Kashmir, Srinagar, 190 006, India*
[2]*Department of Physics, National Institute of Technology, Srinagar, 190 006, India*
[3]*Department of Physics, Govt. Degree College Kulgam, 192 231, India*
[4]*Cluster University Srinagar, Jammu and Kashmir, 190 001, India*
[5]*Department of Physics, University of Notre Dame, Notre Dame, USA*
[6]*iThemba LABS, National Research Foundation, P.O. Box 722, Somerset-West 7129, South Africa*
[7]*Department of Physics, University of Zululand, Private Bag X1001, KwaDlangezwa, 3886, South Africa*
[8]*University of Western Cape, Department of Physics, P/B X17, Bellville, ZA-7535, South Africa*
(Dated: December 8, 2017)

Excited band structures recently observed in ^{156}Dy are investigated using the microscopic triaxial projected shell model (TPSM) approach and the quasiparticle random phase approximation (QRPA) based on the rotating mean-field. It is demonstrated that new observed excited bands, tracking the ground-state band, are the γ-bands based on the excited two-quasineutron configurations as conjuctured in the experimental work.

PACS numbers: 21.60.Cs, 23.20.Lv, 23.20.-g, 27.70.+q

I. INTRODUCTION

A major challenge in nuclear theory is to elucidate the rich band structures observed in atomic nuclei [1]. The phenomenal progress achieved in the experimental techniques in recent years has made it possible to probe the nuclear structure properties at the extremes of spin and isospin. In some heavier nuclei, more than thirty band structures have been identified and some of these bands extend up to angular-momentum of sixty [2–5]. The band structures provide valuable information on the dependence of nuclear properties on excitation energy and angular-momentum. For instance, it is known that pairing correlations are reduced with angular-momentum due to alignment of protons and neutrons in high-j intruder orbitals. The particles or quasiparticles in these high-j and low-Ω orbitals have maximum projection along the rotational axis and demand less collective rotation to generate the angular-momentum. These quasiparticle configurations then become energetically favored and cross the ground-state configuration at a finite angular-momentum, depending on the region.

In a more recent experimental study [6], the high-spin band structures in ^{156}Dy have been populated. The most interesting aspect of this investigation is the observation of the γ-band based on the ground-state up to highest angular-momentum, I=32 observed so far. The excited bands that decay to this γ-band have been proposed to be the γ-bands based on the two-quasiparticle configurations. This interesting proposition of the γ-bands built on the quasiparticle excitations warrants investigations using theoretical approaches.

The γ-band built on the ground-state or vacuum configuration was introduced by Bohr and Mottelson [1], who interpreted these $K^{\pi} = 2^{+}$ bands as a dynamic quadrupole deviation of the nuclear mean-field potential from the axial shape. In the framework of the Unified Model, it is considered as an intrinsic excitation which when combined with the rotational D-function, restores the angular-momentum. Several approaches have been developed to describe this intrinsic excitation in a microscopic way that include quasiparticle phonon [7, 8], multi-phonon [9–12], dynamic deformation [13], the quasiparticle random phase approximation (QRPA) based on the rotating mean-field, which describes the γ-bands based on high-spin yrast levels in a semi-classical way [14–20].

Recently, the microscopic approach of the triaxial projected shell model (TPSM) has been developed to describe the high-spin band structures in transitional nuclei [21–26]. In this approach, the three-dimensional projection method is applied to project out the good angular-momentum states from the triaxial intrinsic states. From the symmetry requirement, the projection from the self-conjugate vacuum state leads to even-K states with K=0,2, 4,... The K=0, 2, 4 states represent the main components of the ground-state, γ- , and $\gamma\gamma$-bands at low spin.

The TPSM approach includes multi-quasiparticle excitations and it is evident from the very construction of the basis configurations that γ- bands can be also built on the quasiparticle configurations. This interpretation is similar to the tidal wave approach, which will be applied to the γ-vibration for the first time in this paper. It describes the γ-vibration as a travelling wave, which corresponds to uniform rotation about the long-axis of the triaxial shape. Using the cranking model, the properties of the γ-vibration are calculated in a microscopic way without introducing any new parameters.

The recent experimental study of ^{156}Dy [6] provided evidence for the existence of a γ-band based on the ground state band up to very high spins and a second γ-band, which is proposed to be built on the s-configuration, which contains two rotational aligned $i_{13/2}$ quasineutrons. The purpose of the present work is to investigate the conjectured γ-bands, based on the quasiparticle excitations, using the TPSM approach as well as in the framework of the traditional approaches based on the rotating mean-field.

As the band structures in ^{156}Dy have been observed up to spin, I=32, where four-quasiparticle configurations are expected to become important, four-neutron and four-proton quasiparticle configurations have been included for the first time in the TPSM basis. The manuscript is organized in the following manner : Section II.A contains brief description of TPSM approach. Details can be found in our earlier publi-

cations [27, 29, 30]. The results obtained from the TPSM calculations are presented and compared with the experimental data in section II.B. In section II.C, nature of γ-bands is analysed. Section III.A discusses the structure of the positive parity bands in the complementary framework of the conventional cranked shell model and its relation to TPSM interpretation. Section III.B reviews the application of the quasiparticle random phase approximation to the γ-vibration in rotating nuclei from the earlier work in the literature. Section III.C contains the tidal wave study of the γ-vibration and discusses its relation to the TPSM. Conclusions are presented in section IV.

II. TRIAXIAL PROJECTED SHELL MODEL APPROACH

A. Extension of the model

For even-even systems, the normal TPSM basis space is comprised of projected 0-qp or qp-vacuum, 2-proton, 2-neutron and 2-proton + 2-neutron quasiparticle configurations. In the present investigation of the band structures in ^{156}Dy, high-spin states have been observed up to I=32 and in order to describe the states above I=20 accurately, it is important to include also 4-neutron and 4-proton quasiparticle configurations. In the present work, we have extended the TPSM basis space to include these four-quaispraticle configuration and the complete basis space employed in the present work is given by

$$\begin{array}{r} \hat{P}^I_{MK}\,|\Phi>; \\ \hat{P}^I_{MK}\,a^\dagger_{p_1}a^\dagger_{p_2}\,|\Phi>; \\ \hat{P}^I_{MK}\,a^\dagger_{n_1}a^\dagger_{n_2}\,|\Phi>; \\ \hat{P}^I_{MK}\,a^\dagger_{p_1}a^\dagger_{p_2}a^\dagger_{n_1}a^\dagger_{n_2}\,|\Phi>; \\ \hat{P}^I_{MK}\,a^\dagger_{n_1}a^\dagger_{n_2}a^\dagger_{n_3}a^\dagger_{n_4}\,|\Phi>; \\ \hat{P}^I_{MK}\,a^\dagger_{p_1}a^\dagger_{p_2}a^\dagger_{p_3}a^\dagger_{p_4}\,|\Phi>, \end{array} \tag{1}$$

where $|\Phi>$ is the vacuum state and the three-dimensional angular-momentum projection operator [31] is given by

$$\hat{P}^I_{MK} = \frac{2I+1}{8\pi^2}\int d\Omega\, D^I_{MK}(\Omega)\,\hat{R}(\Omega) \quad . \tag{2}$$

In the above equation, $\hat{R}(\Omega)$ is the rotational operator in terms of Euler angles. The adopted projected basis space in Eq. 1 is adequate enough to describe the high-spin states observed in ^{156}Dy up to I=32. $|\Phi>$ in the TPSM approach is the triaxial quasiparticle vacuum state and the angular-momentum projection operator in Eq. 2 not only projects out the good angular-momentum, but also states having good K-values. This is achieved by specifying a value for K in the rotational matrix, "D", in Eq. 2.

It is worthwhile to mention that basic strategy in TPSM is similar to that used in the spherical shell model (SSM) approach except that now a deformed basis is employed rather than the spherical one. The deformed potential in TPSM provides an optimum basis to perform the spectroscopic studies of deformed heavier nuclei that are presently beyond the reach of the SSM approach. In the present work, the Wick's theorem is used to evaluate the matrix elements of rotated many-quasiparticle states. This procedure becomes quite involved for more than two-quasiparticles and for identical four-quasiparticle states, considered in the present development, the number of terms in Hamiltonian kernel run into thousands. We are presently in the process of implementing the Pfaffian technique in the TPSM approach to include the higher quasiparticle states as has been recently done in the PSM approach [32, 33].

The projected basis of Eq. 1 is then used to diagonalise the shell model Hamiltonian. As in our earlier studies, we have employed the pairing plus quadrupole-quadrupole Hamiltonian [31, 34–36]

$$\hat{H} = \hat{H}_0 - \frac{1}{2}\chi\sum_\mu \hat{Q}^\dagger_\mu\hat{Q}_\mu - G_M\hat{P}^\dagger\hat{P} - G_Q\sum_\mu \hat{P}^\dagger_\mu\hat{P}_\mu. \tag{3}$$

The QQ-force strength χ is adjusted such that the physical quadrupole deformation ε is obtained as a result of the self-consistent mean-field HFB calculation [31]. The monopole pairing strength, G_M, is of the standard form

$$G_M = (G_1 \mp G_2\frac{N-Z}{A})\frac{1}{A}\,(\text{MeV}), \tag{4}$$

where $-(+)$ is neutron (proton). In the present calculation, we use $G_1 = 20.12$ and $G_2 = 13.13$, which approximately reproduce the observed odd-even mass difference in this region. This choice of G_M is appropriate for the single-particle space employed in the model, where three major shells are used for each type of nucleon ($N = 3,4,5$ for protons and $N = 4,5,6$ for neutrons). The quadrupole pairing strength G_Q is assumed to be proportional to G_M, the proportionality constant being fixed as 0.16. These interaction strengths are consistent with those used earlier for the same mass region [27, 28, 31].

B. COMPARISON WITH EXPERIMENT

TPSM calculations have been performed for ^{156}Dy by constructing the quasiparticle basis space with deformation parameters of $\varepsilon = 0.278$ and $\varepsilon' = 0.105$, which correspond to $\beta = 0.29$ and $\gamma = 20.6^\circ$ in the standard parametrization. The axial deformation parameter has been adopted from the earlier studies [37]. The nonaxial deformation parameter is chosen in such a way that the band-head of the γ-band is reproduced.

The angular-momentum projected energies from 0-qp, 2-qp, and 4-qp configurations, calculated with deformation parameters given above, are depicted in Fig. 1 for ^{156}Dy. The projection from 0-qp state results into $K = 0,2,4,.....$ with no odd-values due to symmetry requirement for the vacuum configuration and give rise to ground-, γ- and $\gamma\gamma-,.....$bands. The band-head of the γ-band is at an excitation energy of 0.98 MeV from the ground- state and the $\gamma\gamma$-band lies at 2.13 MeV.

Fig. 1 illustrates how the non-rotating quasiparticle basis states of the TPSM become entangled with increasing angular-momentum. The ground-state band is crossed by the

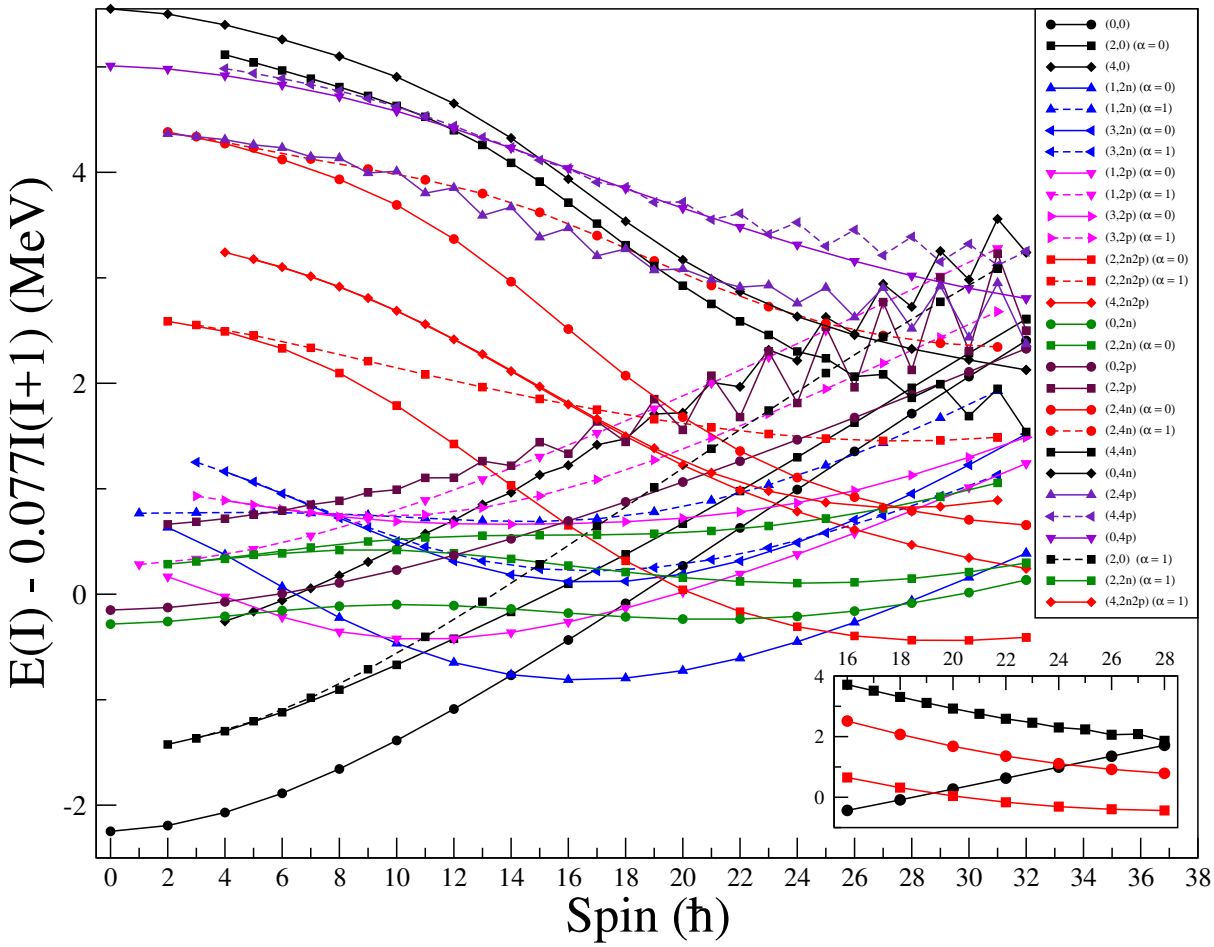

FIG. 1. (Color online) TPSM projected energies, before band mixing, of positive parity states for ^{156}Dy. Bands are labelled by (K, qp numbers) so that the labels (0,0), (2,0), (4,0), (1,2n), (3,2n), (1,2p), (3,2p), (0,2n2p) (2,2n2p) and (4,2n2p) correspond to ground, γ, 2γ, two neutron-aligned state, γ-band on this two neutron-aligned state, two proton-aligned state, γ-band on this two proton-aligned state, two-neutron plus two-proton aligned state, $\gamma-$ and $\gamma\gamma-$ band built on this four-quasiparticle state. The excited K=0 resulting from projection of two-quasineutrons and two-quasiprotons are denoted by (0,2n) and (0,2p), respectively. Some bands, having large signature splitting, are separated into even-spin (labelled as $\alpha = 0$) and odd-spin states (labelled as $\alpha = 1$). The first crossing at I=14 is due to (1,2n) aligned configuration that forms the s-band configuration. The second and third crossings at about I=24 and 28 are due to the aligning 4n configurations with K=2 and 4, respectively. The inset depicts the four-quasiparticle crossings with the ground-state band.

signature, $\alpha = 0$ branch of $(1,2n)$ band, which is a two-quasineutron aligned configuration having K=1, at I=14. Further, the $\alpha = 0$ component of the two-quasiproton aligned band, (1,2p), with K=1 also crosses the ground-state band at I=18. There are also crossings in the excited configuration, for instance, the γ-band built on the two-quasineutron configuration (3,2n) having K=3, crosses the normal γ-band at I=17. As a matter of fact, the lowest odd-spin states in the spin range, I=17-25 originate from this configuration. For spin above I=26, it is noted that four-quasiparticle states (2,2n2p) become yrast. In Fig. 1, the lowest projected K=0 bands, resulting from two-neutron and two-proton quasiparticle structures, are also plotted. These two bands are almost degenerate for low-spin states with band-heads at about 2 MeV excitation energy. For high-spin states however the K=0 two-quasineutron state becomes favoured.

The projected bands from four-neutron and four-proton quasiparticle configurations are also plotted in Fig. 1 and the band structures obtained from these states lie at a higher excitation energy compared to two-neutron+two-proton quasiparticle bands. As is evident from the figure, these configurations remain higher in energy. However, it is noted that the $\alpha = 0$ component of four-neutron quasiparticle state, having K=2, crosses the ground-state band at I=24. The projected band from the K=4 component of the four-neutron state also crosses the ground-state at a higher spin value. On the other hand, the

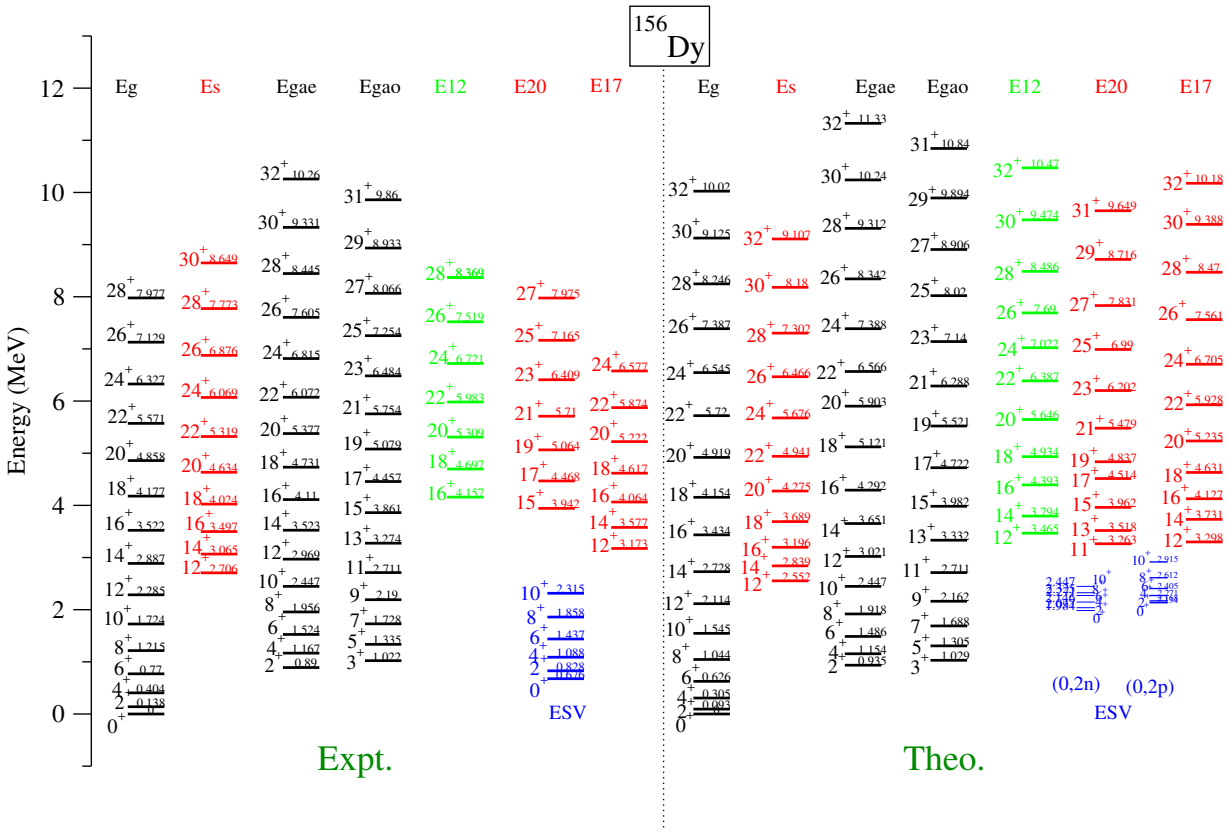

FIG. 2. (Color online) Comparison of the measured positive parity energy levels of ^{156}Dy nucleus [6] and the results of TPSM calculations.

$\alpha = 1$ branch of this configuration and also the four-proton quasiparticle band structures lie at higher excitation energies and don't cross the ground-state band up to the highest studied spin value.

In the next stage of the TPSM study, the lowest projected states, shown in Fig. 1, and many more ($\sim$ 130 for each angular-momentum) are employed to diagonalize the shell model Hamiltonian, Eq. 3. The energies obtained after diagonalization are compared with the measured data in Figs. 2 and 3. The bands are labelled as in the experimental work [6]. The association between the calculated and experimental bands is discussed below. In Fig. 2, we provide the exact energies that can be used for further investigations. Fig. 3 demonstrate that the TPSM calculations describe well the structure of the yrast region. However, the calculated spectrum is too much spread out in energy. As discussed in Sec. III.A, this is probably a consequence of the deformation and the pair gaps being kept constant.

To have a closer comparison between theory and experiment, the excitation energies are subtracted by the rotor contribution and the resulting energies are displayed in Fig. 3 (bottom panels of e and f). It is evident from the two figures that TPSM reproduces the experimental data quite reasonably with the exception for the excited 0^+ band referred to as the SV band. The band-head of the experimentally observed band is at 0.7 MeV excitation and the predicted neutron excited 0^+ is at about 1.9 MeV. Theoretically, it is expected to lie at about 2 MeV which is equal to the excitation energy of the two-quasiparticle states as is evident from Fig. 2. There are some extra correlations, not included in the present work, that bring it down to 0.7 MeV and clearly it is of considerable interest to investigate this problem in detail. It may be of vibrational type, pairing isomer, or a shape coexisting structure. The TPSM does not include corrections of this type.

The correspondence between the theoretical and the experimental band structures plotted in Figs. 2 and 3 is made through the wavefunction analysis as discussed in the following. For some bands, it was possible to identify a few lower angular-momentum states, not observed in the experimental data, through this wavefunction analysis. The dominant components of the wavefunctions of the band structures are depicted in Fig. 4. The ground-state band, shown in the top panel of this figure, has up to I=14 the largest component of $(0,0)$ which is the K=0 projected state from the tri-

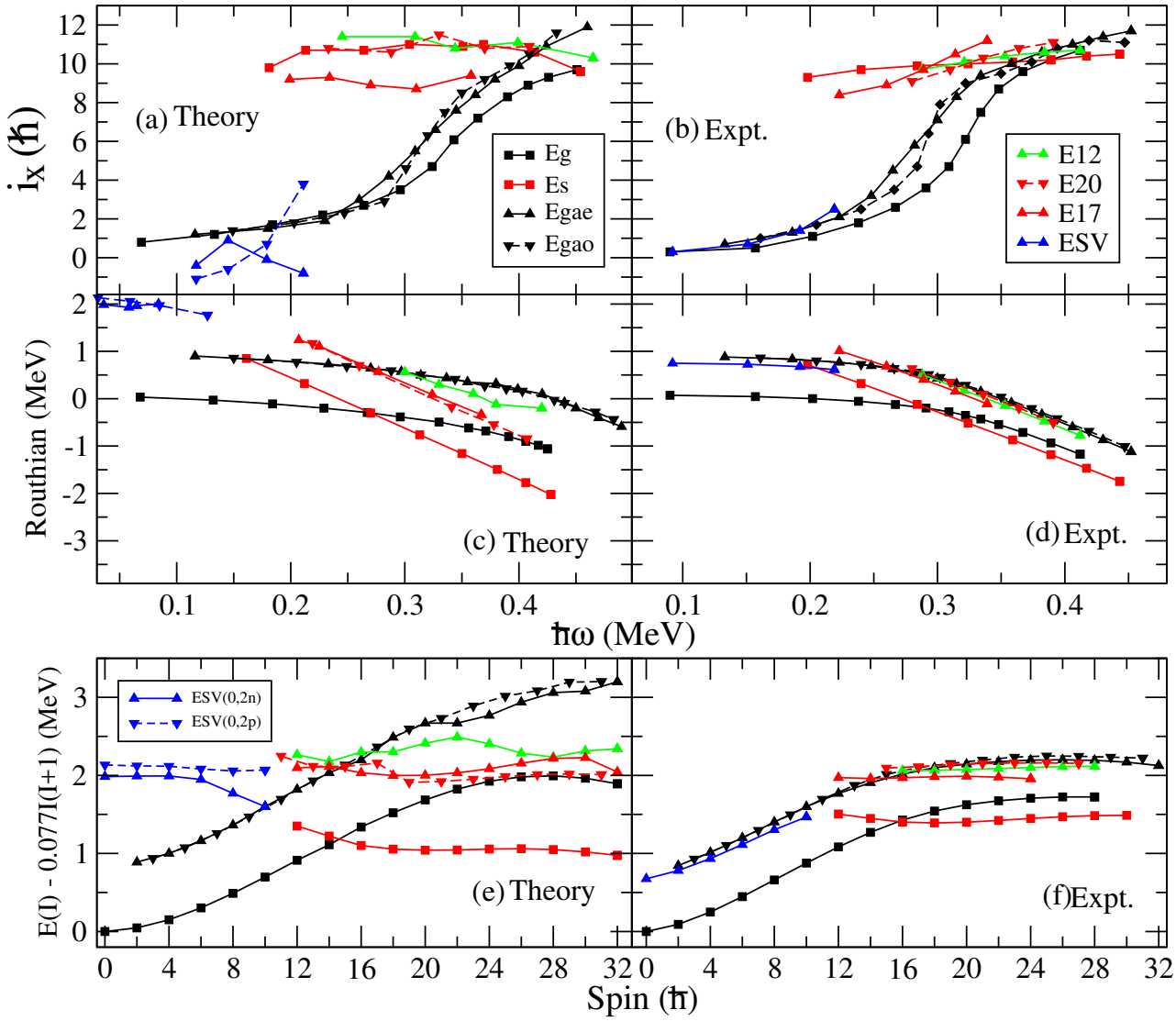

FIG. 3. (Color online) Experimental energies (right panel) of the positive parity bands in ^{156}Dy as reported in Fig. 4 of Ref. [6] compared with the TPSM calculations (left panel). Labeling: Eg - ground state band, Es - s band, Egae - even-spin γ-band, Egao - odd-spin γ-band, ESV - SV band, E12 - band 12, E17 - band 17, E20 band 20. Even-spin states are connected by solid lines odd-spin states by dashed lines. In the upper panel $I_{ref} = \omega \mathcal{J}_0 + \omega^3 \mathcal{J}_1$ is subtracted. In the lower panel $E'_{ref} = -\omega^2 \mathcal{J}_0/2 - \omega^4 \mathcal{J}_1/4$ is subtracted with $\mathcal{J}_0 = 23\hbar^2\text{MeV}^{-1}$ and $\mathcal{J}_1 = 90\hbar^4\text{MeV}^{-3}$.

axial vacuum configuration. It is also evident that the two-quasiproton component, $(1,2p)$, is building up with spin and becomes dominant in the spin region, I=18-22. For I=24 and beyond, four-quasiparticle components are becoming important, in particular, the K=2 four-neutron configuration. Therefore, this band is not really the ground-state band as it has dominant two-quasiparticle and four-quasiparticle configuration for I=18 and beyond. The wavefunction of the s-band, shown in the second panel of Fig. 4, has the largest component from the aligned two-quasineutron state, $(1,2n)$, up to I=24 and beyond this spin value the four-quasiparticle configurations dominate.

The largest component in the wavefunction of the even-spin γ-band, shown in the third panel of Fig. 4, up to I=14 is $(2,0)$ which is the K=2 projected state from the 0-qp configuration. It is also noted that the component $(3,2p)$, which is the γ-band built on the two-proton aligned band, is quite large in spin regime, I=14-18 and above I=18 the s-band configuration, $(1,2n)$, becomes dominant. For the odd-spin γ-band, the composition of the wavefunction is similar to the even-spin branch. The bands 17 and 20, shown in the 5th and 6th panels of Fig. 4, have interesting structures with dominant component from $(3,2n)$, which is the γ-band based on the two-quasineutron configuration.

From the above analysis, the emerging picture for the band structures labelled as 17 and 20 is quite similar to what has

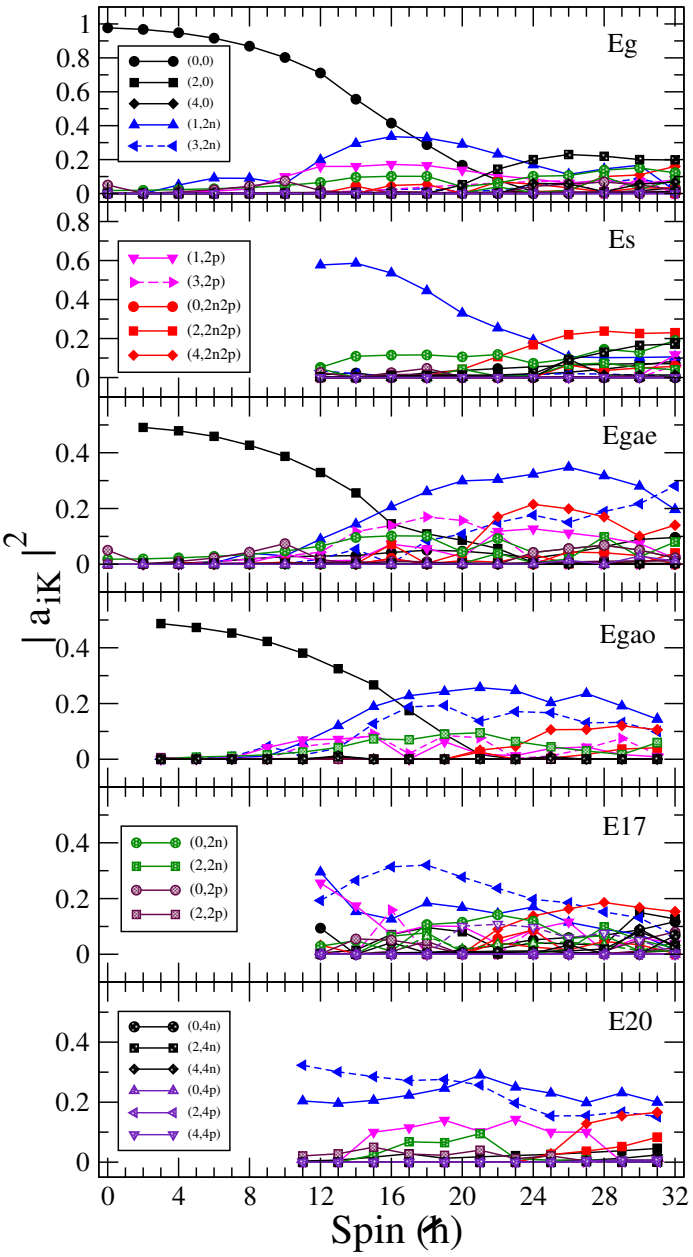

FIG. 4. (Color online) Probability of various projected K-configurations in the wavefunctions of the band structures after diagonalization are plotted for the ^{156}Dy nucleus.

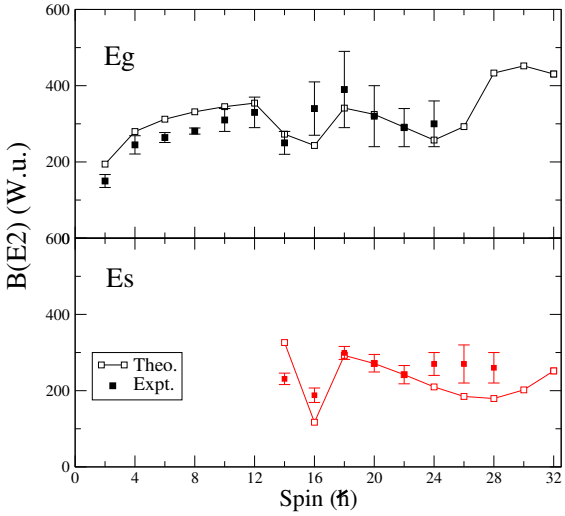

FIG. 5. (Color online) Calculated $B(E2)$ transition probabilities for the ground-state band and the s-band using the TPSM approach. The experimental values have been taken from Refs. [38–40].

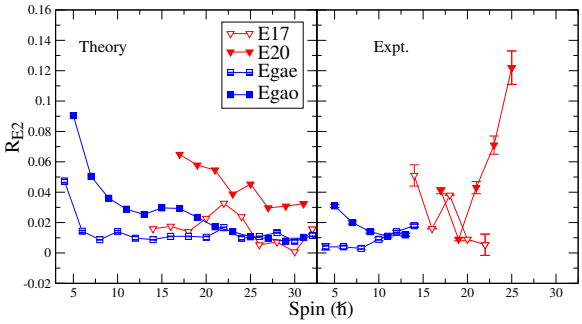

FIG. 6. (Color online) Ratios of the $B(E2)$ values for out-of band to in-band transitions $R_{E2} = B(E2;out)/B(E2;in)$ for the γ decays from the γ-band to the ground-state band and for the γ decays from bands 17 and 20 to the s-band

been proposed in the experimental work [6]. The component $(3,2n)$, which is γ-band built on the two-neutron aligned configuration, is quite dominant in the wavefunctions of the band structures labelled as Band 17 and Band 20. These bands are built on the same intrinsic quasiparticle as that of the s-band of the second panel in Fig. 4, except that these are projected with K=3. It is also evident from Fig. 4 that these are not purely γ-bands built on the two-quasineutron configuration as these also have significant contributions from other configurations. This is related to the inter-band mixing, in particular, for high-spin states and also due to non-orthogonality of the projected states.

Further, it is interesting to note from Fig. 4 that the Even and Odd γ-bands initially have the dominant component $(2,0)$ as expected, however, for intermediate spin-values, the configuration $(3,2p)$ becomes important, which is similar to the ground state band. This has to be the case, otherwise the γ-band would not track the ground state band. This configuration is the γ-band built on the two-quasiproton configuration. The ground-state band is crossed by the normal two-quasiproton configuration and we infer from Fig. 4 that for the γ-band, it is γ-band based on two-quasiproton state that

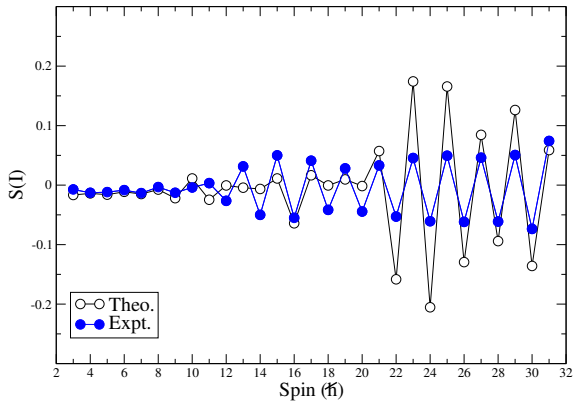

FIG. 7. (Color online) Comparison of observed and TPSM calculated staggering parameter Eq. (5) for the γ-band in ^{156}Dy.

TABLE I. Calculated $M1$ (μ_N^2) units from Egao→Eg and E20→Es of ^{156}Dy nucleus.

Spin (I^π)	Egao→Eg	E20→Es
3^+	0.013	
5^+	0.011	
7^+	0.010	
9^+	0.008	
11^+	0.003	
13^+	0.002	0.124
15^+	0.004	0.122
17^+	0.006	0.071
19^+	0.008	0.029
21^+	0.002	0.017
23^+	0.003	0.009
25^+	0.005	0.005
27^+	0.003	0.007
29^+	0.004	0.001
31^+	0.001	0.002

crosses.

The experimental interpretation of the band structures as γ-bands built on the ground-state and two-quasiparticle configurations is based on the transition probabilities between the bands. The transition probabilities have been calculated in the TPSM approach with the effective charges of 1.5e for protons and 0.5e for neutrons. The $B(E2)$ values for the transition between the ground-state and the s-bands are depicted in Fig. 5 along with the known experimental values. Two dips in the $B(E2)$ curve for the ground-state band is due to the crossing of the two-proton and four-neutron aligned configurations at spin, I=18$\hbar$ and 24$\hbar$, respectively. A small drop in the $B(E2)$ transitions of the s-band at I=14$\hbar$ is due to mixing of (2,2n) and ground-state bands. Further, as in the experimental work, we have also evaluated the ratios R_{E2} of the out-of-band $B(E2;out)$ to the in-band $B(E2;in)$ strengths, where the out-of-band transitions connect the $\gamma-$ band with the ground-state band and bands 17 and 20 with the s-band. [It needs to be added that $B(M1)$ transition probabilities, shown in Table I, are an order of magnitude smaller than $B(E2)$ transitions and hence evaluation of branching ratios with $B(E2)$ values only is justified.] As depicted in Fig. 6, the R_{E2} values for all the bands are of same order of magnitude, supporting the interpretation that band 17 and 20 are the γ-bands built on the s-band configuration. The TPSM reproduces fairly well the experimental values.

The wavefunction of Band 12 for spin states of I=16, 18 and 20 are dominated by two-proton aligned configuration, $(1,2p)$, and above I=24 the wavefunction has predominant contribution from four-quasiparticle states. Clearly, g-factor measurements are needed to probe the intrinsic structures of these band structures.

To examine further the quasiparticle structures of the observed band structures, we have analyzed the alignments of the bands as a function of the rotational frequency and the results are presented in Fig. 3 (top panels, a and b). The observed ground-state band has a gradual increase in the alignment at a rotational frequency of $\hbar\omega = 0.3$ MeV. This increase is also noted in the TPSM calculated alignment, although it is slower than in the experimental data. This increase can be traced to the alignment of four-neutrons having K=2. This configuration crosses the ground-state band at I=24 and becomes the dominant component in the ground-state band above this spin value as is evident from Fig. 4. Both even- and odd-spin members of the γ-band also show an increase in the aligned angular-momentum, which is due to the increasing contribution of $(1,2n)$ component in these band structures.

C. Nature of the γ-bands

Analyzing the collective Bohr-Hamiltonian results, it has been suggested that signature splitting of the γ-band is sensitive to the nature of γ deformation (see e.g the review [41]). The observed pattern is : harmonic γ-vibration about axial shape - both signatures degenerate; γ-independent potential - even spin below odd spin; rigid triaxial potential - odd spin below even spin. To quantify the tendency, the following staggering parameter has been introduced :

$$S(I) = \frac{E(I) - (E(I-1) + E(I+1))/2}{E(2_1^+)}, \qquad (5)$$

which measures the energy of state I relative to the average energy of the two neighbours. Fig. 7 compares the TPSM results with experiment for the γ-band on top of the ground state band. The staggering $S(I)$ is quite small at low spin, which is expected for a well established axial shape. Above I=10 the staggering increases with the even-spin states below the odd ones. The TPSM calculations reproduce observed staggering pattern, as well as the $R_{E2} = B(E2;out)/B(E2;in)$ values, as shown in Fig. 6 and, therefore, account for the nature of the γ-deformation of ^{156}Dy nucleus. The even-spin lower, which is a signature for γ-softness, appears to be in conflict with the assumption of the TPSM of a fixed γ-deformation, which suggests that the criterion based on the Bohr Hamiltonian does not apply for $I > 10$ as the TSPM ratios R_{E2} are consistent with

experiment. Within the TPSM framework, the staggering pattern can be related to the following : for low-even spin states the major components are (2,0) and (2,2p). The two-neutron aligned configuration, (1,2n), becomes important above I=10 as is evident from Fig. 4, showing the wave function probabilities. For the even-spin members of the γ-band, the low-energy even-spin states (1,2n) ($\alpha = 0$) (cf. Fig. 1) have a large probability. For the odd-spin members of the γ-band the high-energy odd-spin states (1,2n) ($\alpha = 1$) (cf. Fig. 1) have a large probability.

Bands 17 and 20 are assigned to the even- and odd-spin members of the γ-band on top of the s-configuration because the basis states (3,2n) $\alpha = 0, 1$ are dominant, where both signatures have nearly the same energy (cf. Fig. 1). As for the γ-band on top of the ground state band, both signatures contain a large (1,2n) component of the respective signature, which energetically prefers the even-spin members.

As seen in Fig. 4, the γ-bands are distributed over multiple basis states. As we shall discuss in the next section, the QRPA treatment of the γ-vibration based on the s-band indicates substantial fragmentation as well. Another reason is the change of the quasiparticle structure caused by rotation. Since the TPSM uses the quasiparticle configurations in the non-rotational potential as a basis, it describes the modification of the quasiparticle structure in the rotating potential by mixing the non-rotating configurations.

III. ROTATING MEAN-FIELD INTERPRETATION

A. Cranked Shell Model

Fig. 2 displays the experimental energies and Fig. 3 the experimental aligned angular-momenta and routhians for the positive parity bands. The simplest-possible interpretation is the Cranked Shell Model (CSM) [42], which associates the bands with quasiparticle configurations in a potential rotating with frequency $\hbar\omega$ about one of its principal axes. Fig. 8 depicts a calculation using the axial Nilsson potential combined with the monopole pair field as described in ref. [42]. The deformation parameters are $\varepsilon = 0.26$ and $\gamma = 0$, which are close to the equilibrium deformation found by means of the Cranked Nilsson-Strutinsky method for the relevant spin range [4]. The pair gaps are $\Delta_p = 1.0$ MeV and $\Delta_n = 0.9$ MeV. The ground state band is represented by the vacuum denoted by 0. Below $\hbar\omega$= 0.15 MeV, it corresponds to all negative-energy quasiparticle routhians occupied. Above it corresponds to the adiabatic continuation of this configuration. The other configurations are denoted by the occupied routhians labelled by the letters (the reflected-through-0 routhians are unoccupied).

Figs. 9 and 10 show the lowest positive parity bands labelled by their quasiparticle configurations. Comparing the CSM calculation with the experiment shown in Fig. 2 and 3, one notices that the crossing between the g- band (configuration 0) and the s-bands (AB) is qualitatively described. The CSM crossing frequency of $\hbar\omega = 0.23$ MeV underestimates the experimental value of $\hbar\omega = 0.28$ MeV, which is a well known deficiency of the CSM. The aligned angular-momenta are of right magnitude. The distance between the two bands after their crossing is overestimated (about 1 MeV in experiment vs. about 2 MeV in the calculation). We attribute this to the assumption of a fixed deformation and fixed pairing gaps. The Cranked Nilsson-Strutinsky calculations of Ref. [4], which assume no pairing and optimize the deformation for each configuration, obtain a more compressed spectrum, close to experiment. The CSM gives two even-spin (ABEF and ABef) and one odd-spin (AC) bands between the s- and the g-bands, where Ref. [6] suggests the experimental location of the two signatures of the γ-band on top of the s-band. The close neighborhood may cause fragmentation of the collective strength among these two-quasiparticle (relative to AB) excitations.

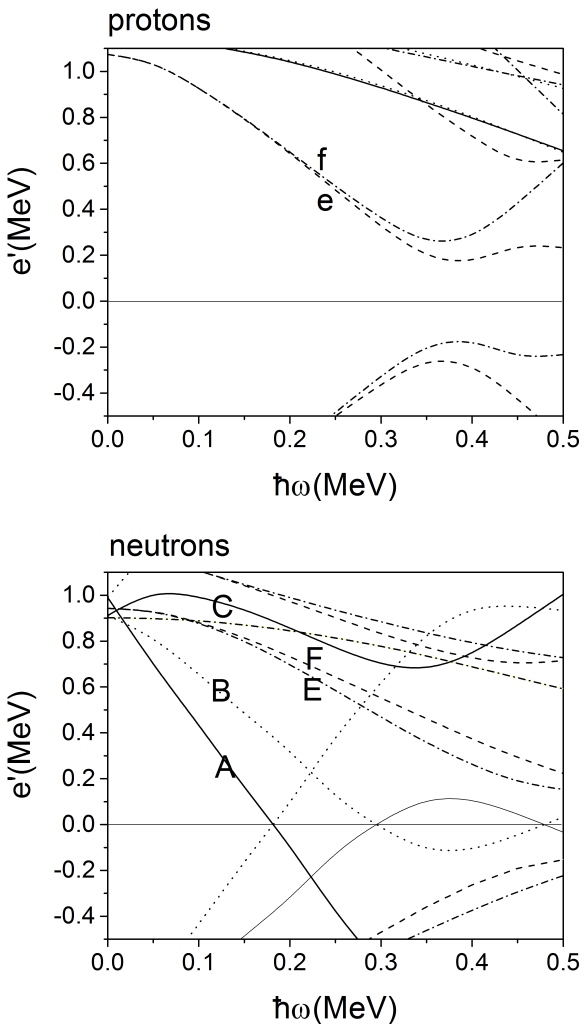

FIG. 8. Quasiparticle routhians for ^{156}Dy.

B. Quasiparticle Random Phase Approximation

Quasiparticle Random Phase Approximation is the standard extension of the mean-field approximation to describe

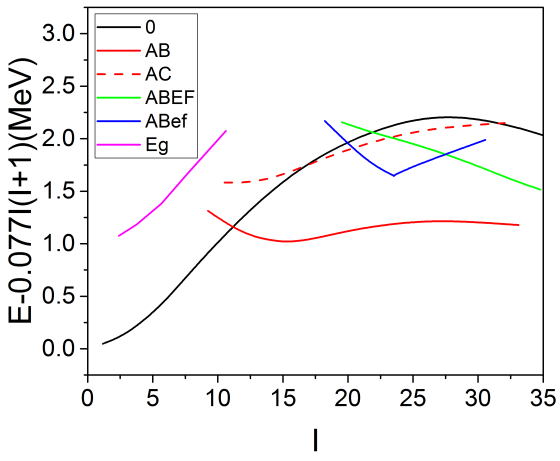

FIG. 9. Energies of the lowest positive parity bands in ^{156}Dy calculated by means of the cranking model. The bands are labeled by the occupied quasiparticles in Fig. 8. Eg is the γ-band calculated by means of the tidal wave approach. Even-spin states are connected by straight lines odd-spin states by dashed lines.

collective excitations. In order to describe the γ-vibrations in rotational nuclei, the authors of Refs. [14–20] applied QRPA to the rotating mean-field and the pairing + quadrupole quadrupole model Hamiltonian, Eq. 3, below with $G_Q = 0$. Since the rotating mean-field conserves signature, the QRPA leads to two independent sets of equations, one for even and the other one for odd spins.

Fig. 11 shows the QRPA results of Refs. [18–20]. The authors used the self-consistency requirement for a harmonic oscillator potential and volume conservation introduced by Bohr and Mottelson [1] to determine the quadrupole deformation and to fix the coupling constant χ. The calculations reproduce very well the experimental energies of the odd-spin branch of the γ-band on top of the g- band. The calculated branching ratios $R_{E2} = B(E2, I \to I-1 : out)/B(E2, I \to I-2 : in) \sim 0.02$ between the transitions out-of and within the γ-band account for the measured ratios [6] (see Fig. 6). Above the crossing between the g- and s- bands (g-band stands for the ground state band and s-band for the two-quasiparticle aligned band), the QRPA solutions are based on the s-band, which is yrast. The three lowest odd-spin solutions are found close together. This suggests that the collective vibrational strength may be fragmented over these states instead of being concentrated in one individual state. The authors quote only the ratio $B(E2, I \to I-1 : out)/B(E2, I \to I-2 : in) \sim 0.04$ for the lowest band. The value is consistent with the widely scattered experimental ratios of band 20 (see Fig. 6), who's excitation energy with respect to the s-band of about 0.75 MeV is somewhat larger than the QRPA value of about 0.60 MeV. The lowest three even-spin QRPA solutions are close together as well, which may lead to fragmentation. The lowest solution lies about 0.2 MeV above yrast, which is substantially lower than the position of band 17, the experimental candidate for the even-spin γ-band. The calculated ratio $B(E2, I \to I-2 : out)/B(E2, I \to I-2 : in) \sim 0.01$ is to be

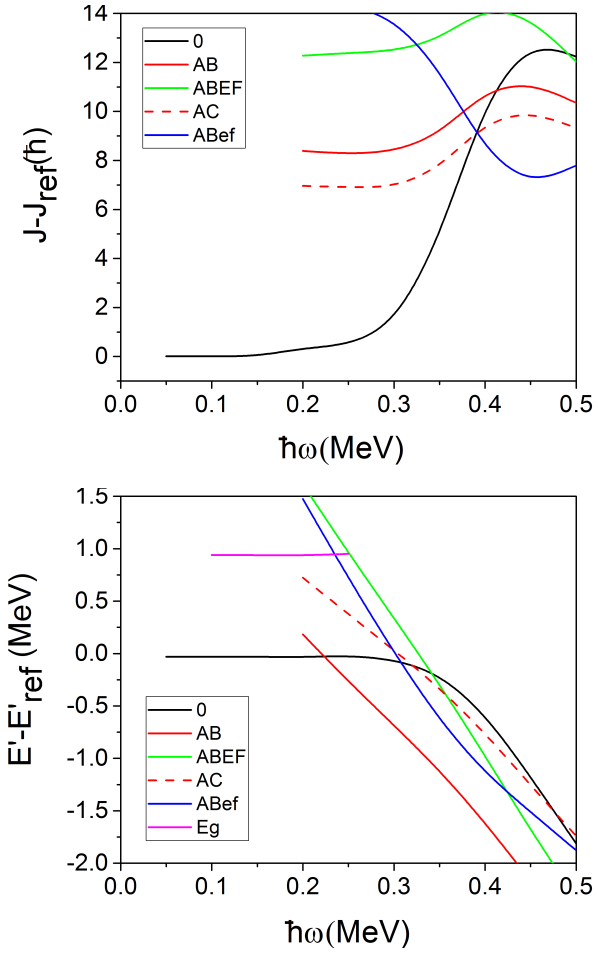

FIG. 10. Upper panel: Angular-momentum expectation values calculated by means of the cranking model relative to the reference. Lower panel: Routhians relative to the reference. Reference as in Fig. 3.

compared with the experimental ratio ~ 0.2.

The QRPA approach becomes unreliable in the vicinity of the crossing of the g- and s- bands. The reason is that g- and s- configurations have different deformations (0 axial and AB triaxial). The cranking model produces a mixing between the configurations, which makes the even-spin QRPA energy approaching zero, which is an artifact. The mixing falsifies the energies of the lowest QRPA even-spin solution already away from the crossing. In contrast to experiment, the even-spin solution (not shown) was found below the odd-spin sequence. The low energy of the even-spin QRPA solutions on top of the s- configuration may be an artifact as well. The authors of Refs. [14–17] avoided these problems by removing the mixing between the g- and s- configurations. For the studied nucleus ^{164}Er both the even-spin and odd-spin QRPA solutions are stable in the crossing region.

As seen in Fig. 11, The QRPA calculations [20] reproduce the experimental energies of the SV band very well. The structure of the QRPA solution is not analyzed in detail. By construction, it has to be a combination of a β-type and a pairing

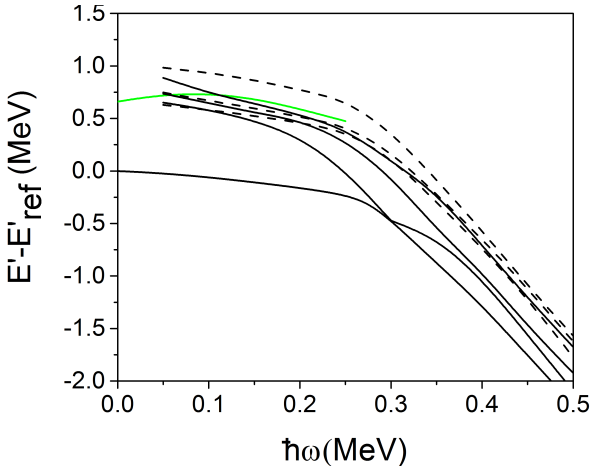

FIG. 11. Routhians of the lowest positive parity bands in ^{156}Dy calculated by means of the QRPA extension of the rotating mean-field derived from the pairing + quadrupole quadrupole model Hamiltonian. Even-spin states are connected by straight lines odd-spin states by dashed lines. Green line depicts the QRPA results for the β band, i.e., the band based on the 0_2^+ state. Figure has been prepared using the results of Refs. [18–20]. Reference energy is as in Fig. 3.

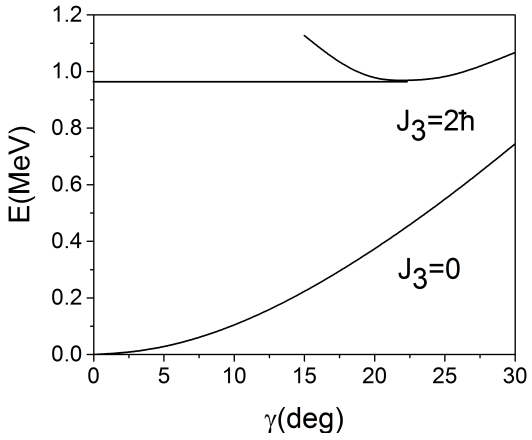

FIG. 12. Energy of the $J_3 = 0$ and $J_3 = 2\hbar$ calculated by the shell correction version of the cranking model.

vibration.

C. Tidal Wave Approach

The tidal wave concept has been developed to describe the yrast sequence of near-spherical and transitional nuclei [43, 44]. It can be directly applied to the γ-degree of freedom. The γ-vibration carries $2\hbar$ of angular-momentum along the symmetry axis. Classically, the sequence n = 1, 2, 3, ... of aligned γ phonons is represented by a wave travelling around the symmetry axis 3 with the angular velocity $\hbar\omega_\gamma = E_\gamma/2$ carrying the angular-momentum $J_3 = K\hbar = 2n\hbar$. In the co-rotating frame, the wave is represented by a constant γ-deformation, which increases $\propto \sqrt{n}$. For a travelling wave the angular-momentum and energy increase by increasing the amplitude while the rotational frequency stays constant. For a triaxial rotor the states above the yrast sequence are also generated by adding quanta of angular-momentum along the axis with the smallest moment of inertia. The difference to the tidal wave is that the angular-momentum and energy increase by increasing the rotational frequency while the deformation stays constant. Obviously, the concept also comprises the intermediate cases of an anharmonic γ-vibration and a soft triaxial rotor.

It is important to realize that it is not possible to distinguish between a triaxial rotor and a harmonic γ-vibration, as long as one considers only the first excited (K=2) band. In both cases an angular-momentum of $J_3 = 2\hbar$ is generated by a γ-deformed shape rotating about the 3-axis. To differentiate one has to take the next (K=4) band into consideration. The K-dependence of ω_γ is indicated by the level distance, $\hbar\omega_\gamma = (E_\gamma(K) - E_\gamma(K-2))/2$. In the case of a vibration, the level distance is the same and so is the frequency ω_γ for $K = 2$ and $K = 4$ bands. To view it as a rotation, $\omega_\gamma = K/\mathscr{J}$ implies $\mathscr{J}(K=4) = 2\,\mathscr{J}(K=2)$. Because $\mathscr{J} \propto \gamma$, one must have deformation parameter $\gamma(K=4) = \sqrt{2}\gamma(K=2)$, which means $E_\gamma(K=4) = 2E_\gamma(K=2)$. In the case of the rigid triaxial rotor, $\gamma(K=4) = \gamma(K=2)$ and with a fixed moment of inertia $\mathscr{J}$, the energy $E_\gamma = K^2/2\,\mathscr{J}$, which means that $\omega_\gamma(K=4) = 2\omega_\gamma(K=2)$ implying $E_\gamma(K=4) = 4E_\gamma(K=2)$. This explains why the TPSM approach [27] which operates with a fixed γ deformation describes the first excitations of γ vibrational type in ^{156}Dy, which has an axial shape at the moderate spins of interest in this communication.

For the first time, we apply the Tidal Wave concept to the γ vibration in a quantitative way. The travelling wave is described by cranking the triaxial potential about the long-axis with the frequency ω_γ. The total angular-momentum $J_3(\omega_\gamma, \gamma) = \langle 0|j_3|0\rangle$ and the total routhian $E'(\omega_\gamma, \gamma)$ are calculated by means of the shell correction version of the cranking model as described in Ref. [45]. The total energy $E(J_3 = 2, \gamma) = E'(\omega_\gamma, \gamma) + \omega_\gamma J_3(\omega_\gamma, \gamma)$ is minimized with respect to γ, where ω_γ is fixed by requiring $J_3(\omega_\gamma, \gamma) = 2\hbar$.

The calculation is carried out for the vacuum configuration $|0, \omega_\gamma\rangle$, which corresponds to all negative energy quasiparticle routhians occupied. Like for rotation about the short-axes 1, 2 shown in Fig. 8, the continuation of the configuration to frequencies $\hbar\omega_\gamma > 0.3$ MeV leads into the region where the negative- and positive-energy quasiparticle encounter. The cranking model generates an unphysical mixing of the 0 configuration with high-j configurations (AB for example). In order to remove the mixing, the low-frequency routhians are extrapolated using fourth-oder polynomials, which corresponds to third-order perturbation theory with respect to ω_γ. The Harris parametrization :

$$J_3 = \omega_\gamma \mathscr{J}_0 + \omega_\gamma^3 \mathscr{J}_1, \quad E' = E_0 - \frac{\omega_\gamma}{2}\mathscr{J}_0 - \frac{\omega_\gamma^4}{4}\mathscr{J}_1 \quad , \quad (6)$$

is fitted to the cranking values in the range $0 \le \hbar\omega_\gamma \le 0.1$ MeV. The extrapolation very well reproduces the cranking

calculations up to the region where the mixing with the high-j configurations sets in.

Fig. 12 shows that the energy with $J_3 = 0$ is minimal for $\gamma = 0$, which indicates that the γ-band has the character of a tidal wave. For $J_3 = 2\hbar$ the minimum lies at $\gamma = 22.5^\circ$, which is the amplitude of the wave travelling about the symmetry axis. The energy of the minimum $E_\gamma = 0.97$ MeV is somewhat larger than the experimental energy of the γ-band head of $E(2_2^+) = 0.890$ MeV. The energy $2\hbar\omega_\gamma$=0.91 MeV corresponding to angular velocity of the wave at the minimum of $\omega_\gamma = 0.456\text{MeV}/\hbar$, remarkably well reproduces the experimental 2_2^+ energy. Up to spin I=10 the coupling of the γ-band to other bands is relatively weak. Accordingly, the band-head energy is added to the g-band in Fig. 9. Using the semi-classical expression given in Ref. [45], the cranking calculations provide the $B(E2,\omega)_{TAC}$ values. A rough estimate of the reduced transition probability $B(E2, 2_2^+ \to 0_1^+)$ is given by the semi-classical expression for $J_3 = 1\hbar$, because the latter is proportional to J_3. The calculated ratio

$$\frac{B(E2, 2_2^+ \to 0_1^+)}{B(E2, 2_1^+ \to 0_1^+)} = \frac{B(E2, \omega_3(J_3 = 1\hbar)_{TAC}}{B(E2, \omega_1(J_1 = 2\hbar)_{TAC}} \qquad (7)$$

of 0.043 is close to the experimental ratio of 0.048 [46]. .

The tidal wave approach reproduces the properties of γ-band head remarkably well without introducing any new parameters. This approach becomes equivalent to the QRPA approach when the two approaches are applied to the pairing + quadrupole quadrupole Hamiltonian and the linear extrapolation is used for $J_3(\omega_3)$ instead of the third order Harris expression. The TPSM, also describes the γ-excitations by assuming a constant γ-deformation. Instead of the semi-classical cranking model it generates the travelling wave by means of quantal angular-momentum projection. The γ-deformation is considered as a parameter that is adjusted to reproduce the excitation energy of the γ-band on top of the ground state band. The value of $\gamma = 20.6^\circ$ is close to 22.5° calculated by the tidal wave approach. As discussed above this does not mean that ^{156}Dy has a rigid triaxial shape. As long as only the first excited γ-band is of interest there is no way to decide whether the triaxiality is static or dynamic. The wavelength of the first excitation is too large to resolve details of the potential in the γ-degree of freedom that separate a harmonic travelling wave from a rigid rotor.

IV. CONCLUSIONS

The recently observed band structures in ^{156}Dy have been interpreted in the framework of the TPSM approach and QRPA based on the rotating mean-field. The γ-band built on the ground state band is well reproduced by the TPSM, in particular, the staggering pattern above $I = 10$, which within the collective model indicates the even-I-low pattern, corresponding to the γ-softness limit. The TPSM analysis strongly supports the interpretation proposed in the experimental work that two excited bands are the γ-bands based on the neutron s-band. This is the first detailed confirmation of γ-bands based on the rotational aligned two-quasineutron configurations, which have been suggested in the framework of QRPA. It would be quite interesting to apply the recently developed state-of-the-art approaches [47–50] to investigate the γ-bands built on the quasiparticle excitations.

V. ACKNOWLEDGEMENTS

S. J. would like to acknowledge MHRD (Govt. of India) for providing the financial support to carry out the research work. Two of us (S. N. T. M. and J. F. S.-S.) would like to acknowledge grants from the National Research Foundation (NRF) of South Africa. S. F. acknowledges support by the US Department of Energy grant No. DE-FG02-95ER4093.

[1] A. Bohr and B. R. Mottelson, *Nuclear Structure*, Vol. II (Benjamin Inc., New York, 1975).
[2] J. D. Morrison et al., Europhys. Lett. **6**, 493 (1988).
[3] J. Simpson et al., J. Phys. **G**, 13 235 (1987).
[4] F. G. Kondev et al., Phys. Lett. **B 437**, 35 (1998).
[5] J. Ollier et al., Phys. Rev. **C 83**, 044309 (2011).
[6] S. N. T. Majola et al., Phys. Rev. **C 91**, 034330 (2015).
[7] V. G. Soloviev and N. Yu. Shirikova, Z. Phys. **A 301**, 263 (1981).
[8] V. G. Soloviev, *Theory of Atomic Nuclei:* Quasiparticles and Phonons (Institute of Physics, London, 1992).
[9] J. Leandri and R. Piepenbring, Phys. Rev. **C 37**, 2779 (1988).
[10] M. K. Jammari and R. Piepenbring, Nucl. Phys. **A 487**, 77 (1988).
[11] H. G. Borner and J. Joli, J. Phys. **G 19**, 217 (1993).
[12] D. G. Burke and P. C. Sood, Phys. Rev. **C 51**, 3525 (1995).
[13] K. Kumar, *Nuclear Models and Search for Unity in Nuclear Physics* (Universitetforlaget, Bergen, Norway, 1984).
[14] Y. R. Shimizu and K. Matsuyanagi, Prog. Theor. Phys. **67**, 1637 (1982).
[15] Y. R. Shimizu and K. Matsuyanagi, Prog. Theor. Phys. **67**, 1641 (1982).
[16] Y. R. Shimizu and K. Matsuyanagi, Prog. Theor. Phys. **70**, 144 (1982).
[17] Y. R. Shimizu and K. Matsuyanagi, Prog. Theor. Phys. **72**, 799 (1982).
[18] J. Kvasil and R. G. Nazmitdinov, Phys. Rev. **69**, 031304(R) (2004).
[19] J. Kvasil and R. G. Nazmitdinov, Phys. Lett. B **650**, 331 (2007).
[20] R. G. Nazmitdinov and J. Kvasil , J. Exp. Th. Phys, **105**, 926 (2007).
[21] S. Jehangir, G.H. Bhat, J.A. Sheikh, R. Palit, and P.A. Ganai, Nucl. Phys. **A 968**, 48 (2017).
[22] J. Marcellino, E.H. Wang, C. J. Zachary, J. H. Hamilton, A. V. Ramayya, G. H. Bhat, J. A. Sheikh, A. C. Dai, W. Y. Liang, F. R. Xu, J. K. Hwang, N. T. Brewer, Y. X. Luo, J. O. Rasmussen, S. J. Zhu, G. M. Ter-Akopian and Yu Ts. Oganessian, Phys.

Rev. **C 96**, 034319 (2017).
[23] R. Palit, G. H. Bhat and J. A. Sheikh, Eur. Phys. J. **A 53**, 90 (2017).
[24] A. Navin, M. Rejmund, S. Bhattacharyya, R. Palit, G. H. Bhat, J. A. Sheikh, A. Lemasson, S. Bhattacharya, M. Caamaño, E. Clément, O. Delaune, F. Farget, G. De. France and B. Jacquot, Phys. Lett. **B 767**, 480 (2017).
[25] J. A. Sheikh, G. H. Bhat, W. A. Dar, S. Jehangir and P. A. Ganai, Phys. Scr. **91**, 063015 (2016).
[26] G. H. Bhat, J. A. Sheikh, Y. Sun and R. Palit, Nucl. Phys. **A 947**, 127 (2016).
[27] J. A. Sheikh and K. Hara, Phys. Rev. Lett. **82**, 3968 (1999).
[28] Y. Sun, K. Hara, J. A. Sheikh, J. G. Hirsch, V. Velazquez, and M. Guidry, Phys. Rev.**C 61**, 064323 (2000).
[29] J. A. Sheikh, G. H. Bhat, Y. Sun, G. B. Vakil, and R. Palit, Phys. Rev. **C 77**, 034313 (2008).
[30] J. A. Sheikh, G. H. Bhat, R. Palit, Z. Naik, and Y. Sun, Nucl. Phys. **A 824**, 58 (2009).
[31] K. Hara and Y. Sun, Int. J. Mod. Phys. **E 4**, 637 (1995).
[32] L.-Jun Wang, Y. Sun, T. Mizusaki, M. Oi, and S.K. Ghorui, Phys. Rev. **C 93**, 034322 (2016).
[33] L.-Jun Wang, F.-Qi Chen, T. Mizusaki, M. Oi, and Y. Sun, Phys. Rev. **C 90**, 011303 (2014).
[34] G. H. Bhat, W. A. Dar, J. A. Sheikh, and Y. Sun, Phys. Rev. **C 89**, 014328 (2014).
[35] J. A. Sheikh, G. H. Bhat, Yan-Xin Liu, Fang-Qi Chen and Y. Sun, Phys. Rev. **C 84**, 054314 (2011).
[36] G. H. Bhat, J. A. Sheikh, Y. Sun and U. Garg, Phys. Rev. **C 86**, 047307 (2012).
[37] S. Raman, C. H. Malarkey, W. T. Milner, C. W. Nestor, Jr., and P. H. Stelson, Atom. Data Nucl. Data Tables **36**, 1 (1987).
[38] O. Möller et al., Phys. Rev. **C 74**, 024313 (2006).
[39] A. Dewald et al., Eur. Phys. J. **A 20**, 173 (2004).
[40] P. Petkov et al., **C 68**, 034328 (2003).
[41] S. Frauendorf, Int. J. Mod. Phys. E **38**, 1541001 (2015).
[42] R. Bengtsson and S. Frauendorf, Nucl. Phys. A **327**, 139 (1979).
[43] S. Frauendorf, Y. Gu, J. Sun, Int. J. Mod. Phys. E 20, 465 (2011), arXiv-id: 0709.0254 (2010)..
[44] A.D. Ayangeakaa et al. Phys. Rev. Lett. **110**, 10250 1(2013).
[45] S. Frauendorf, Nucl. Phys. A **677**, 115 (2000).
[46] National Nuclear Data Center, Brookhaven National Laboratory, http://www.nndc.bnl.gov.
[47] J. L. Egido, M. Borrajo, and T.-R. Rodriguez, Phys. Rev. Lett. **116**, 052502 (2016).
[48] Y. Utsuno, N. Shimizu, T. Otsuka, T. Yoshida, Y. Tsunoda, Phys. Rev. Lett. **114**, 032501 (2015).
[49] Y. F. Niu, Z. M. Niu, G. Colo, and E. Vigezzi, Phys. Rev. Lett. **114** 142501 (2015).
[50] K. Nomura, T. Niksic, and D. Vretenar, Phys. Rev. **C 93**, 054305 (2016).